Damage analysis of a crack layer

J. BOTSIS
Department of Civil Engineering, Mechanics and Metallurgy, University of Illinois at Chicago, PO Box 4348, Chicago, IL 60680, USA

Damage analysis of a crack layer in polystyrene is carried out by employing optical microscopy and principles of quantitative stereology. The results show that, within the quasistatic phase of crack layer propagation, the average crazing density, along the trailing edge of the active zone, is constant. This is consistent with a self-similarity hypothesis of damage evolution employed by the crack layer theory. The average crazing densities within the active zone and along its trailing edge are found to be practically equal. A layer of constant crazing density, adjacent to the crack planes, accompanies the crack during its quasi-static growth. This suggests that: (1) a certain level of crazing density should be reached, around the crack tip, prior to crack advance; (2) the specific energy, associated with this 'core' of damage, could be considered as a Griffith's type energy. The results are in favour of certain hypotheses adopted by the crack layer theory.

1. Introduction

During the process of fatigue fracture, failure initially ensues on the submicroscopic level through damage accumulation which results from the interaction of the applied load and the local microdefects. Damage interaction yields a macroscopic crack (crack initiation) which propagates in a quasi-static fashion to dynamic fracture. Whereas the transition to dynamic fracture is a global instability phenomenon, crack initiation and its subsequent quasi-static propagation are the results of local instability.

Recent experimental work in polystyrene (PS) has demonstrated that damage in the form of crazes precedes crack initiation. When crazing density reaches a certain level, crack initiation is observed [1]. During the quasi-static phase of propagation, an intense zone of crazing precedes and surrounds the crack [1]. It is found that the width of the crazing zone increases by almost an order of magnitude from initiation up to the transition to dynamic fracture. This phase of propagation is well described by the crack layer (CL) theory [2].

Dynamic cracking is accompanied by a craze zone as well as in the quasi-static phase. The only difference is in the pulsating fashion in which damage propagates during the dynamic phase [3].

The scope of this paper is limited to the analysis of damage distribution, during rectilinear quasi-static CL propagation, using PS as a model material. This material, besides being transparent, preserves damage patterns induced during fracture for a relatively long period of time. The experiments are aimed at studying the evolution of the crazing distribution. Subsequently, some of the hypotheses of the CL theory [4, 5] are examined. The results contained herein consist of both macroscopic and microscopic studies and their relationships. Macroscopic studies are primarily involved with the evolution of the surrounding damage

layer. Microscopic studies consist of quantitative damage analysis obtained from highly magnified optical micrographs and employ principles of quantitative stereology [6, 7]. For completeness, the effect of damage on fracture toughness is considered.

2. Experimental procedures

The material which is used in this investigation is plane isotropic PS of 0.25 mm thickness obtained from Transilwrap Corporation (Cleveland, OH). A 60° V-shaped single edge notch of 1 mm in depth is milled into the specimens which are of 80 mm gauge length and 20 mm in width. Details of specimen preparation can be found in [1]. Tension–tension fatigue experiments are performed on a 20 kN capacity electrohydraulic-closed loop MTS machine in a laboratory atmosphere using a sinusoidal waveform loading at a frequency at 0.2 Hz and load ratio of 0.2. A travelling optical microscope is employed to register crack propagation and the evolution of the surrounding damage. The energy release rate is calculated as K^2/E where E is the elastic modulus of the material which is determined experimentally. The stress intensity factor K is calculated using the formula $K = \sigma_{max}(\pi l)^{1/2} f(l/B)$ where σ_{max} is the maximum stress of the fatigue cycle, l is the crack length, B is the width of the specimen and $f(l/B)$ is a correction factor [8]. Crack propagation and the history of damage evolution are obtained from micrographs taken without interrupting the experiment. Crazing distribution is determined from micrographs of transverse and longitudinal thin sections (about 25–30 μm thick) which are prepared by standard metallographic and polishing procedures [6].

3. Background

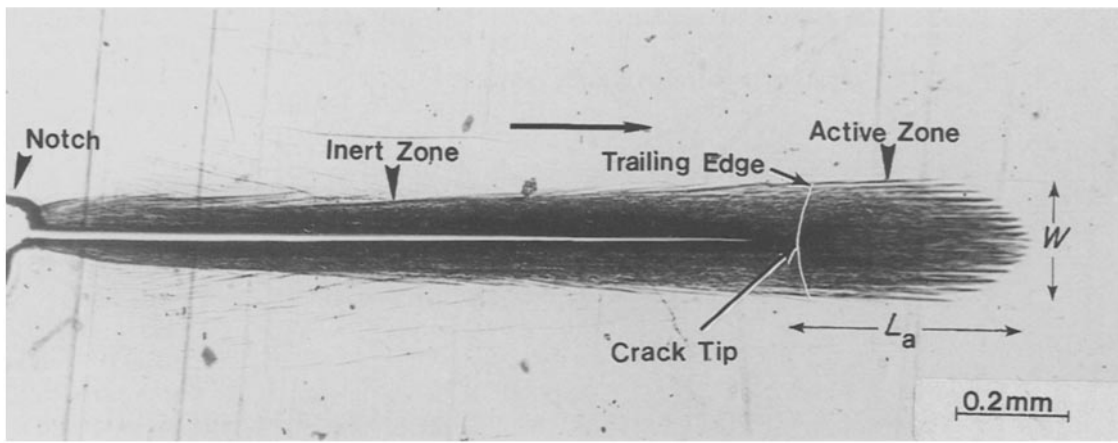In most engineering materials, crack growth is accompanied by damage. The latter consists of crazes [1, 9],

Figure 1 A well developed CL during quasi-static propagation horizontal arrow shows the direction of propagation [1].

shear bands [10], martensitic transformation [11], slip planes [12], etc. Although, the dimensions of the zone within which damage disseminates can be very small compared to the crack length, the energy expended on damage formation may be orders of magnitude higher than that expended on the formation of crack surfaces [13].

The crack layer theory has been advanced to model fracture processes as observed [4, 5]. Within this theory, the crack and the surrounding damage is considered as a macroscopic entity, that is, a crack layer (CL). A general view of a CL in PS grown under fatigue loading is shown in Fig. 1 [1].

A material point X represents a small volume V of actual material. Crazes in V may be characterized by their number, location with respect to the centre of V, characteristic size and orientation. When there is no change in orientation, during propagation, a scalar parameter is sufficient to characterize damage. For example, one can introduce damage density ϱ, as mm^2/mm^{-3} or as $g\,mm^{-3}$. The former represents the amount of middle planes of the damage elements (i.e., microcracking) per unit volume of the material and the latter represents the amount of transformed material (i.e., martensitic transformation).

In terms of the damage parameter ϱ, the CL consists of the area, which surrounds the main crack, within which $\varrho > 0$ (if a certain level of damage preexists then a reference damage density should be established for CL determination). The part of a CL within which $\dot{\varrho} > 0$ is called its active zone. The part of a CL complementary to the active zone is the inert zone. The boundary between the two is the trailing edge (Fig. 1).

A hypothesis of self-similarity of damage evolution

has been adopted by the CL theory [4, 5], namely, the value of the damage density ϱ, at a point X of the active zone at time t, coincides with that at the corresponding point in the initial ($t = 0$) configuration of the active zone the correspondence is given by a time-dependent affine transformation of the space variables [5, 14]. Thus the movements of the active zone may be represented as a translation and rotation of a rigid body and deformation.

Within the framework of irreversible thermodynamics, the rates of these movements are considered as thermodynamic fluxes. The forces conjugate to the fluxes appear in the expression for the global entropy production rate [4, 5]. Translation of the active zone coincides with crack extension. The translational force X^{tr}, is [5]:

$$X^{tr} = \gamma^* R_1 - A_1 \tag{1}$$

Here, γ^* is the specific enthalpy of damage, a material constant, R_1 is the resistance moment which represents the amount of new damage formed per unit crack advance and A_1 is the total potential energy release rate for active zone advance per unit crack length increment. Whereas A_1 expresses the energy available, $\gamma^* R_1$ represents the energy required for unit CL translation. Therefore, Equation 1 expresses the energy barrier for CL extension.

For rectilinear CL propagation R_1 and A_1 are [5]:

$$R_1 = -\langle\varrho\rangle w + \partial_l e R_0 + \partial_l V_{ij}^d R_{ij} \tag{2}$$

$$A_1 = J_1 + \partial_l e M + \partial_l V_{ij}^d N_{ij} \tag{3}$$

where $\langle\varrho\rangle$ is the damage density in $mm^2 mm^{-3}$ averaged over the trailing edge of the active zone, w is the width of the CL (Fig. 1), e is an expansion
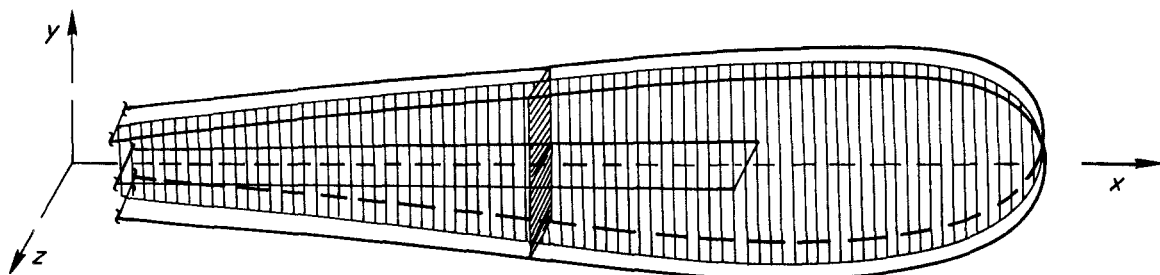

Figure 2 An illustration of CL topology. Shadowed zones indicate the cross sections used for analysis of crazing distribution.
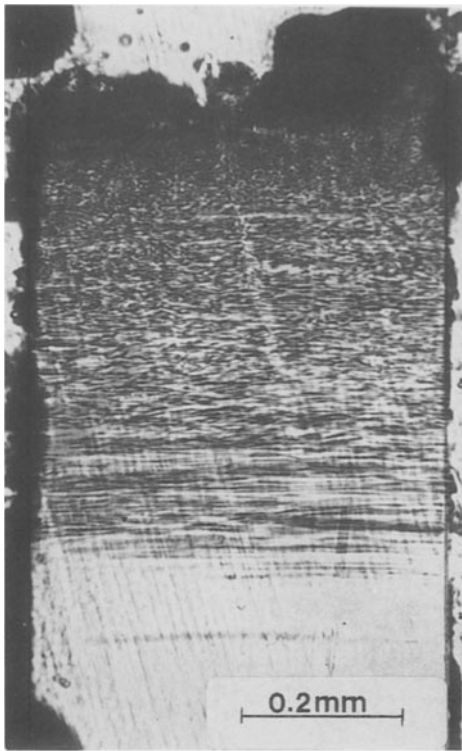
2019

Figure 3 A typical transverse section of the lower part of a CL.

parameter, R_0 and R_{ij} are the resistance moments for expansion and distortion of the active zone, respectively, J_1, M and N_{ij} are the energy release rates for active zone translation, expansion and distortion, respectively. The superscript d denotes the deviatoric component of the deformation tensor$_{ij}$ and ∂ stands for the partial derivative with respect to crack length. The minus sign in the first term of the right-hand side (RHS) of Equation 2 reflects that the direction of the outward normal on the trailing edge of the active zone is opposite to the crack growth direction [4, 5]. Apparently, the CL theory implies that, under particular load history, the average damage density over the trailing edge $\langle \varrho \rangle$, remains constant during the entire quasi-static CL propagation.

As A_1 approaches $\gamma^* R_1$ (Equation 1) the crack speed tends to infinity and corresponds to the transition to dynamic fracture, at which

$$A_{1c} = \gamma^* R_{1c} \qquad (4)$$

where A_{1c} and R_{1c} are the energy release rate and resistance moment for CL translation at critical CL propagation. Thus the theory stipulates that the critical energy release rate is the product of a material constant, γ^*, and a history-dependent parameter, R_{1c}.

In general, two stages of active zone growth are distinguished. First is active zone expansion and distortion which instantaneously follows crack excursion. This is reflected in the second and third terms of the RHS of Equation 2. The second stage is slow damage growth following crack advance and is reflected in the first term of the RHS of Equation 2. Although, in our fatigue experiments only the second part is measurable, the first part is seemingly small and its contribution to A_1 and R_1 is neglected. Thus Equations. 2–4 reduce to

$$|R_1| \cong \langle \varrho \rangle w \qquad (5)$$

$$A_1 \cong J_1 \qquad (6)$$

$$A_{1c} \cong \gamma^* \langle \varrho \rangle w_c \qquad (7)$$

where w_c is the width at critical CL propagation. For PS, the total energy release rate A_1 evaluated from conventional load–displacement curves appears to be close to the elastic energy release rate G_1 [15]. This can be understood in view of the small size of the active zone with respect to the crack length ($l_a/l \sim w/l \ll 1$). Hence for PS, A_1 in Equation 6 can be further approximated by the elastic energy release rate G_1. For polycarbonate, however, the active zone is comparatively large and A_1 can only be evaluated from the evolution of load–displacement curves [16].

4. Results

Information about the distribution of crazes within the CL are obtained through optical microscopy studies of transverse and longitudinal thin sections (25–50 μm thick) of a CL. A typical micrograph of the lower half of a section along the yz plane (Fig. 2) is shown in Fig. 3. While crazes are oriented perpendicular to the axis of the load application, crazing density is uniformly distributed along the thickness direction and monotonically increases towards the fracture surface (directions z and y, respectively, Fig. 2).
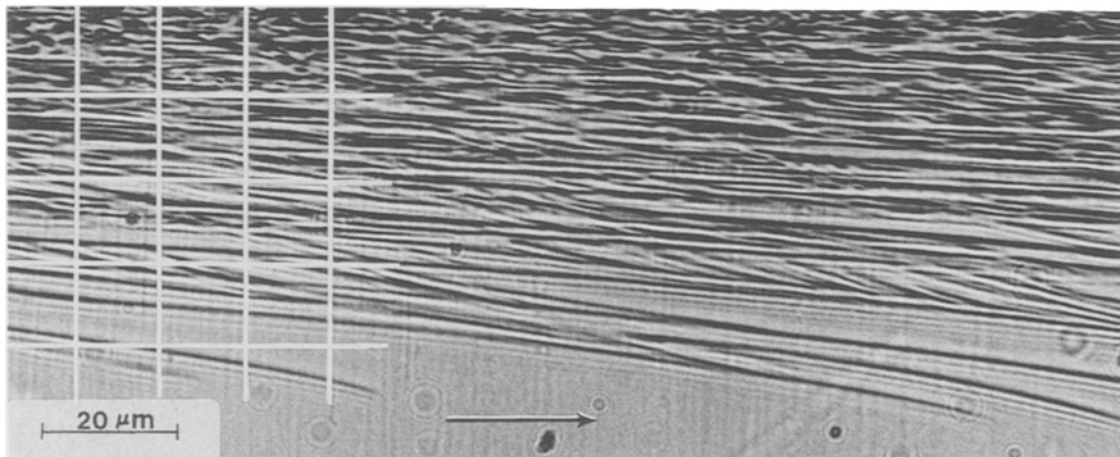
Since crazing density is homogeneously distributed

Figure 4 Transmission optical micrograph of a portion of a CL. The squares indicate the mesh for crazing density measurements.
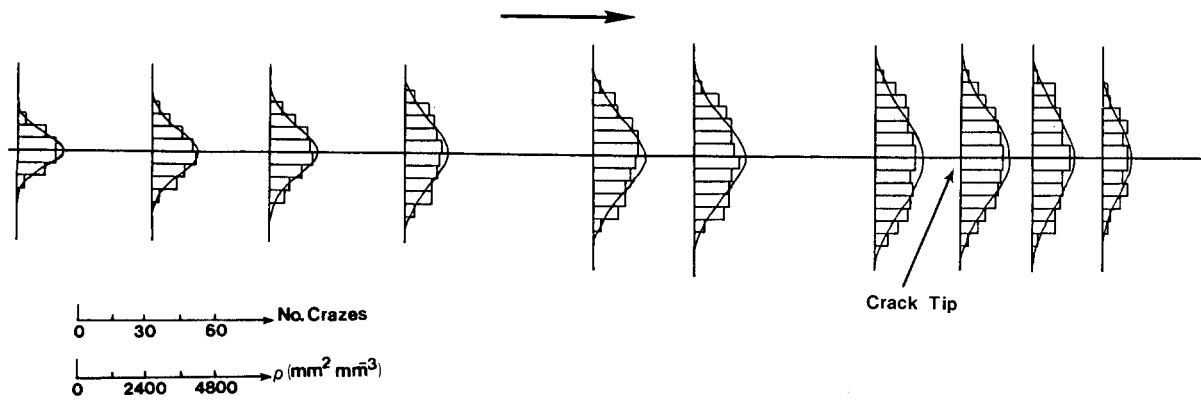
No. Crazes
0 30 60

ρ (mm^2 mm^{-3})
0 2400 4800

Figure 5 Histograms of crazing density within a CL and their normal distribution approximations.
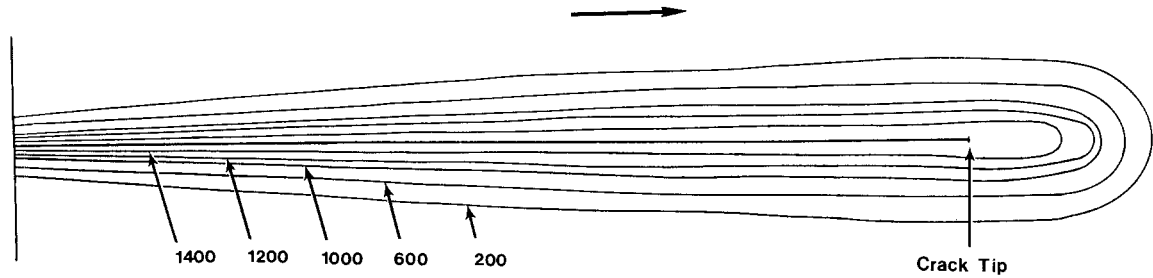

1400 1200 1000 600 200   Crack Tip

Figure 6 Contours of equal level of crazing density in mm^{2}mm^{-3}.

along the thickness direction, a section of a CL parallel to the plane of the specimen (xy-plane) adequately represents crazing distribution within a CL. For our measurements, a section is obtained by standard metallographic thinning of a well developed CL (xy-plane) grown at $\sigma_{mean} = 16$ MPa. Figure 4 exhibits such a micrograph of a portion of the CL. Here, individual crazes can be distinguished within the CL.

From micrographs similar to that shown in Fig. 4, histograms of crazing density against the distance perpendicular to crack direction are obtained using the methodology which is widely used in material science [7].

The micrograph is covered by a mesh of rectangles whose size is approximately an order of magnitude less than the area of interest. In every rectangle, the number of intersections of the crazes with a vertical test line is counted. We then use the formula:

$$\varrho = \frac{nbT}{abT} \tag{8}$$

where ϱ (mm^2 mm^{-3}) represents the amount of area of craze midplanes per unit volume, n is the number of intersections of crazes with the vertical test line at the respective rectangle, a, b are the height and width of a rectangle, respectively, and T is the specimen thickness.

Crazing densities are calculated along the trailing edge and within the active zone. It should be noted that, at any time T, the trailing edge is the only portion of the active zone along which damage density remains unaltered as CL evolves. This edge is approximated here by a straight segment perpendicular to the crack propagation direction.
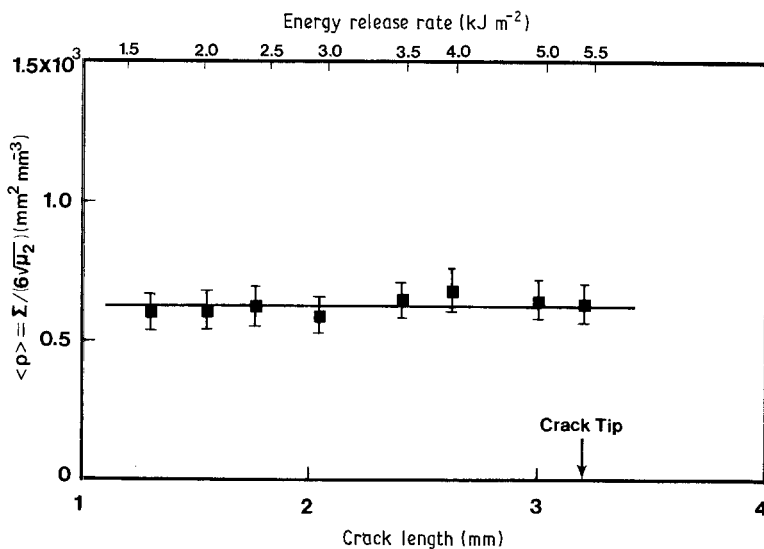

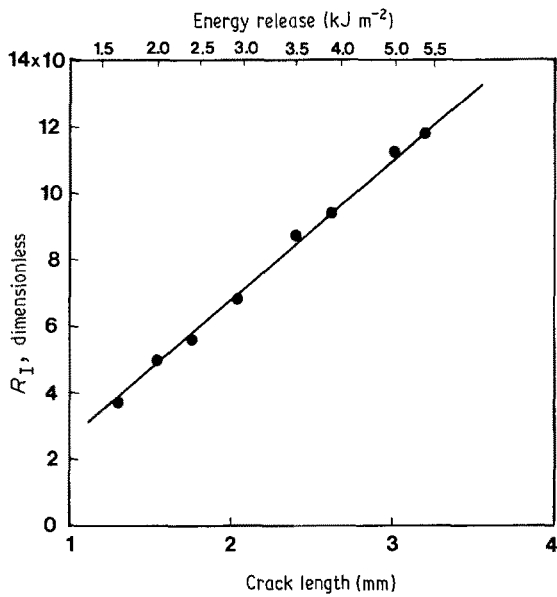*Figure 7* Variation of the average crazing density with the crack length.

Figure 8 Variation of the resistance moment (Equation 5) with crack length.

Measurements along these segments yield the histograms shown in Fig. 5, for eight locations within the inert zone and two locations within the active zone, respectively. Subsequently, using the mean and variance of these histograms we approximate them by the normal distribution curve (Fig. 5) [17]. Based on the normal distribution approximations, contours of equal crazing density are plotted in Fig. 6.

Figure 7 represents the average craze density $\langle \varrho \rangle$, in vertical cross sections at eight locations along the crack path. The values of $\langle \varrho \rangle$ are taken as the ratio of the total amount of crazes Σ, to six times the standard deviation $\sqrt{\mu_2}$, of the respective histograms (Fig. 5).

According to Equation 5, the resistance moment for CL translation R_1, is the product of the average crazing density along the trailing edge of the active zone and its respective width. Variation of R_1 with the crack length is shown in Fig. 8.

A crazing density averaged over the active zone is also estimated by dividing the entire active zone into vertical sections of equal width and calculating the average craze density for each of them. The average of these densities results in $\langle \varrho_0 \rangle = 630 \, \text{mm}^2 \text{mm}^{-3}$.

Optical microscopy observations on thinned sec-

tions show that within a CL, one can distinguish a zone of highly intense crazing adjacent to the crack planes. A portion of this "core" of damage is shown in Fig. 9. The density of crazing within the "core" is plotted in Fig. 10 as a function of the crack length.

Figure 11 displays the lower portion of the transverse sections at critical CL propagation for two experiments performed under $\sigma_m = 16$ and $10.7 \, \text{MPa}$, respectively [1]. While the width at critical CL propagation w_c, is practically the same (Fig. 11), the critical energy release rate measured under $\sigma_m = 10.7 \, \text{MPa}$ is almost twice the critical energy release rate measured under $\sigma_m = 16 \, \text{MPa}$ [1]. Using Equation 7, it has been shown [2] that:

$$R_{Ic}^{(1)} / R_{Ic}^{(2)} \cong A_{Ic}^{(1)} / A_{Ic}^{(2)}.$$

This experimental evidence supports the proposition of the CL that γ^* is a material constant.

5. Discussion

The data which are shown in Fig. 7 demonstrate that, within experimental error, the average crazing density $\langle \varrho \rangle$, along the trailing edge of the active zone is constant. This agrees with the implications of the self similarity hypothesis of damage evolution [14]. Analysis of the same experimental data has shown that craze distribution stays the same up to a uniform dilation from section to section [14]. This results in the constancy of the average craze density along the trailing edge. Consequently, in order to evaluate the resistance moment (Equation 5), we need the average crazing density at any section within the quasi-static CL propagation and the evolution of the active zone width (Fig. 8).

The constancy of the crazing density within the "core" of damage suggests that a certain level of damage density, around the crack tip, is required for quasi-static crack growth. Its constancy may be a manifestation of the invariant shape of the stress distribution in the vicinity of the crack tip (the crack length is only scaling the stress which is manifested in the spread of the damage). This density of damage may further be looked upon as the critical level for local instability.

Equation 4 can alternatively be written as [18]:
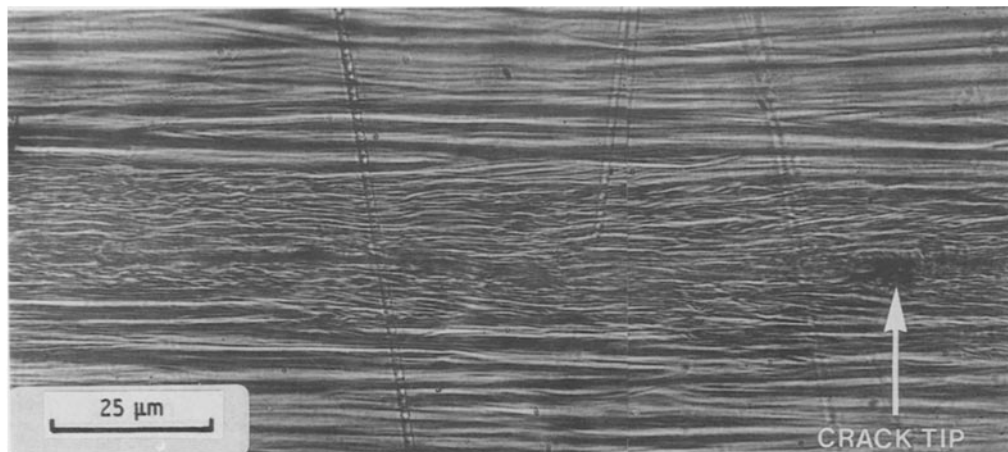
$$A_{Ic} = \gamma_0^* + \gamma^* R_{Ic}^r$$

Figure 9 Transmission optical micrograph taken in the vicinity of the crack path.
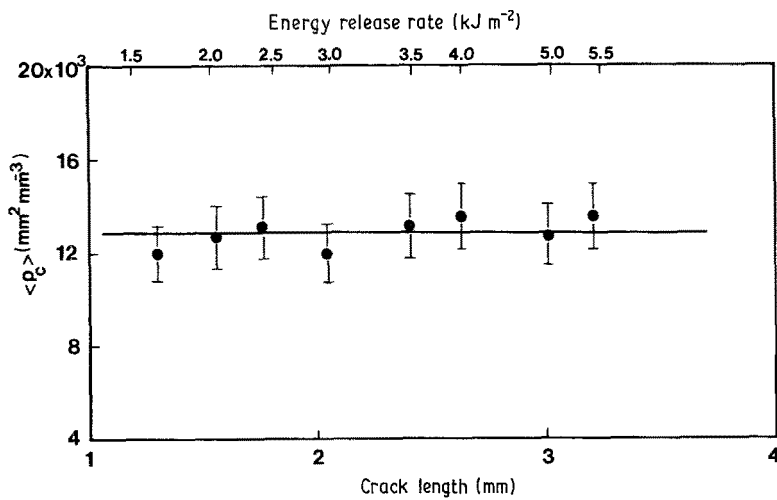
The first term $\gamma_0 = \gamma^* R_I^c$ is a Griffith's type energy associated with either the crack surfaces or, in more general sense, a "core" of damage (Fig. 9). During CL growth γ_0 should remain constant. The results presented in Fig. 10 suggest that this energy term is constant during quasi-static crack growth. The second term $\gamma^* R_{Ic}$ describes the loading history dependence of A_{Ic}.

6. Conclusions

1. The average crazing density remains constant along the trailing edge of the active zone.

2. The data suggest that a critical level of crazing density should be reached at the crack tip prior to crack growth.

3. There is a Griffith's type energy associated with a "core" of intensive damage which remains constant during the quasi-static phase of CL propagation.

Acknowledgement

References

1. J. BOTSIS, A. CHUDNOVSKY and A. MOET, *Int. J. Fracture* **33** (1987) 263.
2. *Idem, ibid.* **33** (1987) 277.
3. J. BOTSIS and A. CHUDNOVSKY, *ibid.* **33** (1987) R67.
4. A. CHUDNOVSKY and A. MOET, *J. Mater. Sci.* **20** (1985) 630.
5. A. CHUDNOVSKY, *J. Appl. Mech.* in press.
6. S. A. HOLIK, R. P. KAMBOUR, D. G. FINK and S. Y. HOBBS, in "Microstructural Science," Vol. 7, edited by LeMay, Fallon and McCall (Elsevier North Holland, 1979) p. 357.
7. E. E. UNDERWOOD, in "Quantitative Stereology" (Addison-Wesley, Reading, MA, 1970) p. 23.
8. H. TADA, P. C. PARIS and G. P. IRWIN, in "The Stress Analysis of Crack Handbook" (Del Research Corporation, Hellertown, PE, 1975) p. 210.
9. A. CHUDNOVSKY, A. MOET, R. J. BANKERT and M. T. TAKEMORI, *J. Appl. Phys.* **54** (1983) 5562.
10. M. T. TAKEMORI and R. P. KAMBOUR, *J. Mater. Sci.* **16** (1981) 1108.
11. G. A. EVANS and A. H. HEMER, *J. Amer. Ceram. Soc.* **63** (1980) 241.
12. A. CHUDNOVSKY and M. BESSENDORF, in "Crack Layer Morphology and Toughness Characterization in Steels", NASA Report 168154.
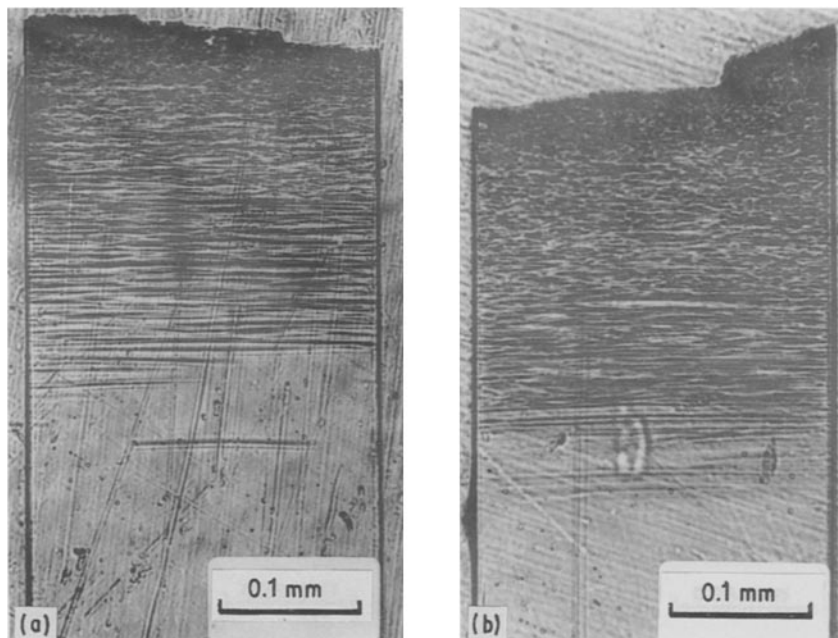13. N. HADDAOUI, A. CHUDNOVSKY and A. MOET,

Figure 11 Optical micrographs taken at critical CL propagation for two loading levels: (a) $\sigma_m = 16$ MPa, (b) $\sigma_m = 10.7$ MPa.

ACS Organic Coating and Applied Science Proceedings **49** (1983) 117.

14. J. BOTSIS and B. KUNIN, *Int. J. Fracture* **35** (1987) RS1.
15. J. BOTSIS, *Polymer* **29** (1988) 457.
16. N. HADDAOUI, A. CHUDNOVSKY and A. MOET, *ibid* **27** (1986) 1377.
17. P. R. BEVINTON, in "Data Reduction and Error Analysis for the Physical Sciences" (McGraw-Hill, New York, 1968).
18. A. CHUDNOVSKY, in "Crack Layer Theory", NASA Report 174634, March 1984.